Available online at www.sciencedirect.com
SCIENCE DIRECT®
Journal of Nuclear Materials 351 (2006) 269–284
journal of nuclear materials
www.elsevier.com/locate/jnucmat

Microstructure of neutron-irradiated iron before and after tensile deformation

S.J. Zinkle [a,*], B.N. Singh [b]

[a] Oak Ridge National Laboratory, P.O. Box 2008, Oak Ridge, TN 37831-6138, USA
[b] Risø National Laboratory, Post Box 49, DK4000 Roskilde, Denmark

Abstract

Tensile specimens of pure Fe were neutron irradiated at 50–70 °C in three fission reactors to displacement dose levels of 0.0001–0.79 displacements per atom (dpa). Irradiated specimens were characterized using transmission electron microscopy (TEM). Visible defect clusters were not detectable by TEM for doses below ~0.001 dpa. Both the density and average size of the dislocation loops increased with increasing dose level. Spatially heterogeneous rafts of dislocation loops lying predominantly on {1 1 1} habit planes were visible for doses above ~0.2 dpa. A high density of small cavities (number density $>10^{24}$ m^{-3}, ~1 nm diameter) was detected following irradiation to 0.79 dpa. The neutron irradiation led to an increase in the yield stress and a decrease in the uniform elongation as a function of increasing dose. Examination of specimens after tensile deformation revealed localized deformation in the form of cleared dislocation channels. Relatively few channels were formed in the uniform elongation region of the gage section. Dislocation channels on multiple slip systems were observed in the deformation region near the fracture surface, presumably due to the multiaxial stress state produced during necking and fracture of the tensile specimen.

1. Introduction

Ferritic steels are used for the pressure vessels of all commercial nuclear power plants, and ferritic/martensitic steels containing 2.25–12%Cr are leading candidates for the structures and pressure vessels of proposed fusion and Generation IV fission reactors [1–4]. There is therefore considerable international research to understand the effects of neutron irradiation on the physical and mechanical properties of ferritic/martensitic steels [1,5]. These physical and mechanical property changes are driven by microstructural changes induced by neutron irradiation. Experimental data on the effects of neutron irradiation on the microstructure of pure iron (coupled with comparable studies on model alloys and complex steels) are useful for understanding the fundamental physical phenomena that are responsible for the property degradation that may occur due to irradiation in steels.

Previous studies on Fe following neutron irradiation near room temperature have reported significant hardening and concomitant reduction in tensile elongation [5–8]. The microstructure of the neutron-irradiated Fe specimens consisted of submicroscopic hardening centers at low doses, and a

* Corresponding author. Tel.: +1 865 576 7220; fax: +1 865 241 3650.
E-mail address: zinklesj@ornl.gov (S.J. Zinkle).

0022-3115/$ - see front matter © 2006 Elsevier B.V. All rights reserved.
doi:10.1016/j.jnucmat.2006.02.031

moderate concentration of small defect clusters at doses above 0.001–0.1 displacements per atom (dpa) [5,7–11]. Due to the small size of the defect clusters in Fe irradiated near room temperature, detailed analyses of the loop nature and configuration have generally not been performed on as-irradiated specimens. Loop analyses performed on Fe following post-irradiation annealing (to increase the defect cluster size) have reported a mixture of primarily interstitial near-edge-type dislocation loops with predominantly $a/2\langle 1\,1\,1\rangle$ Burgers vectors and a smaller concentration of $a\langle 0\,0\,1\rangle$ loops [5,9]. Neutron irradiation of Fe at temperatures above 250 °C has been reported to produce interstitial edge-type dislocation loops with mainly $a\langle 0\,0\,1\rangle$ Burgers vectors and a small concentration of $a/2\langle 1\,1\,1\rangle$ loops [12,13].

The present study was initiated in order to investigate the effect of neutron irradiation near room temperature on the microstructure of pure Fe over a wide (four orders of magnitude) range of dose. The microstructures of irradiated Fe specimens were examined before and after tensile testing in order to investigate the effect of irradiation on deformation mechanisms.

2. Experimental procedure

Two different types of high-purity polycrystalline Fe were used in this study. Specimens irradiated in the High Flux Isotopes Reactor (HFIR) at Oak Ridge National Laboratory were prepared from 99.995% purity foil obtained from Johnson-Matthey. The major impurities from the vendor chemical analysis were 8.3 ppm Si, 8.3 ppm Co, 3.5 ppm S, 2.9 ppm Ni, 2 ppm N, 1.9 ppm Cr, 1.5 ppm Cr, 1.5 ppm Cu, 115 ppm O, and 15 ppm C. The cold-worked foil was recrystallized in vacuum ($\sim 10^{-7}$ Torr) at 600 °C for 0.5 h prior to irradiation, resulting in an average grain size of 33 μm. Specimens irradiated in the DR-3 reactor at Risø National Laboratory and the BR-2 reactor in Mol, Belgium were prepared from cold-worked 99.99% purity foil obtained from Goodfellow. The major impurities in the vendor analysis for this foil were 15 ppm Si, 10 ppm Al, 8 ppm Cr, 7 ppm Mo, 4 ppm Co, 4 ppm Cu, 3 ppm Mn, 3 ppm P, 3 ppm B, 2 ppm S, 2 ppm Ni, and 90 ppm C. After machining, these specimens were vacuum annealed ($\sim 10^{-6}$ Torr) at 650 °C for 2 h, and the final grain size was ~30 μm. The HFIR specimens were irradiated as miniature sheet tensile specimens with an overall length of 17 mm, and gage dimensions of $8 \times 1.5 \times 0.25$ mm. The gage dimensions of tensile specimens irradiated in the DR-3 and BR-2 reactors were $7 \times 3 \times 0.25$ mm. Tensile testing was performed at Risø at 70 °C in a vacuum of $<10^{-2}$ Pa at a strain rate near 1.2×10^{-3} s^{-1}.

The neutron irradiations were performed in the HFIR, DR-3 and BR-2 mixed spectrum fission reactors at irradiation temperatures of 50–70 °C. The HFIR irradiation at 70 °C spanned four orders of magnitude in fluence, 7.2×10^{20}–4.7×10^{24} n/m^2, $E > 1$ MeV which corresponds to displacement damage levels of 1.2×10^{-4}–0.79 dpa, respectively. A recent reanalysis of the calculated damage in Fe for the utilized HFIR irradiation positions resulted in a 10% increase compared to the previously reported maximum damage level of 0.72 dpa [14] for these specimens. The irradiation flux was constant for all of the HFIR irradiations, with a value of 4×10^{18} n/m^2 s ($E > 1$ MeV) or a damage rate of 7×10^{-7} dpa s^{-1}. The corresponding HFIR thermal neutron flux was 2.2×10^{19} n/m^2 s. Duplicate Fe tensile specimens were placed face to face inside of 0.125 mm thick high purity annealed aluminum envelopes (to prevent corrosion in the reactor coolant water) that were vacuum-sealed by electron beam welding. The sealed envelopes were loaded into a perforated hydraulic rabbit capsule that could be moved via the HFIR hydraulic rabbit tube facility in and out of the HFIR target region for periods of time ranging from 180 s to 326 h, producing displacement damage levels of 0.00012, 0.001, 0.01, 0.1 and 0.79 dpa. The HFIR hydraulic tube water pressure of 31 atmospheres ensured good thermal contact of the specimens and aluminum envelope. The DR-3 and BR-2 irradiations at 50–60 °C were focused on intermediate fluences ranging between 1.1 and 2.2×10^{24} n/m^2, $E > 1$ MeV, corresponding to 0.2 and 0.4 dpa. The displacement damage rate for the DR-3 and BR-2 irradiations was ~4 to 5×10^{-8} dpa s^{-1}.

The irradiated microstructure before and after tensile deformation at 70 °C (1.2×10^{-3} s^{-1} strain rate in vacuum) was observed in a JEOL 2000FX transmission electron microscope (TEM) operating at 200 keV, using a combination of bright field and weak beam dark field imaging. Unfortunately, the 0.1 dpa HFIR tensile specimens were damaged during disassembly and were not available for tensile or TEM analysis. The defect cluster density was determined from the slope of plots of the areal density versus foil thickness. The local foil thickness

was measured using thickness fringes in weak beam dark field images. Three different regions of broken tensile specimens were utilized for the microstructural characterization. The as-irradiated microstructure was obtained from examination of the end tab regions of broken tensile specimens. The deformation microstructure in the gage section was observed both in the uniform strain regions and near the fracture surface in order to investigate potential differences of uniaxial versus multiaxial stress states on deformation behavior. Some preliminary results on the as-irradiated microstructure of HFIR-irradiated Fe were previously reported [14].

3. Results

3.1. As-irradiated microstructure

Fig. 1 summarizes the typical weak beam dark field microstructures for pure iron irradiated in HFIR to doses of 0.0001–0.79 dpa. Defect clusters were not visible in the 0.0001 dpa specimen (resolution limit of ~0.5 nm). A low density of small defect clusters with sizes near the TEM resolution limit was detected in the 0.001 dpa specimen. Defect clusters were easily visible in the higher dose specimens using standard bright field and weak beam dark field imaging techniques. The measured network dislocation density in as-irradiated specimens increased slightly with increasing dose from a value of $\sim 10^{12}$ m^{-2} in unirradiated Fe to $\sim 8 \times 10^{12}$ m^{-2} in the 0.79 dpa specimen.

The measured visible loop density and size are summarized in Figs. 2 and 3, respectively. The size and density both monotonically increase with increasing dose above 0.0001 dpa up to the maximum damage level investigated (0.79 dpa). The visible defect cluster density changed from 1×10^{21} to 6×10^{22} m^{-3} as the dose increased from 0.001 to 0.79 dpa. Over the same dose range, the mean visible defect cluster diameter increased from 1 nm to 4 nm. The corresponding maximum observed cluster diameter increased from 1.5 to 8 nm over this dose range (clusters as small as the TEM detection limit of ~0.5 nm were observed at all doses). Fig. 2 also compares defect cluster density results from some previous fission neutron- and 600 MeV proton-irradiated Fe TEM studies [7–9,15,16]. Compared to previous studies, the observed defect cluster density was higher and the average defect cluster size was smaller in the present study. The scatter in reported density data is likely due to differences in impurity contents in 'pure' Fe (particularly interstitial solute) [5,9], as well as experimental difficulties in detecting small clusters in magnetic iron that introduces considerable astigmatism to TEM images.

At high doses, there was a tendency for the visible defect clusters to assemble into small groups. The threshold dose for this dislocation loop alignment in the pure Fe specimens examined in this study, commonly referred to as 'raft formation' [17], was ~0.3 to 0.4 dpa. The raft formation was well developed at 0.79 dpa. Fig. 4 shows the dislocation loop raft microstructure for a beam direction of $\langle 1\,1\,1 \rangle$ in thin and thick foil regions in an iron specimen irradiated to 0.79 dpa. The spatial heterogeneity associated with the loop raft formation is superimposed upon a homogeneous background distribution of small loops. Most of the visible loops were clustered along {1 1 1} habit

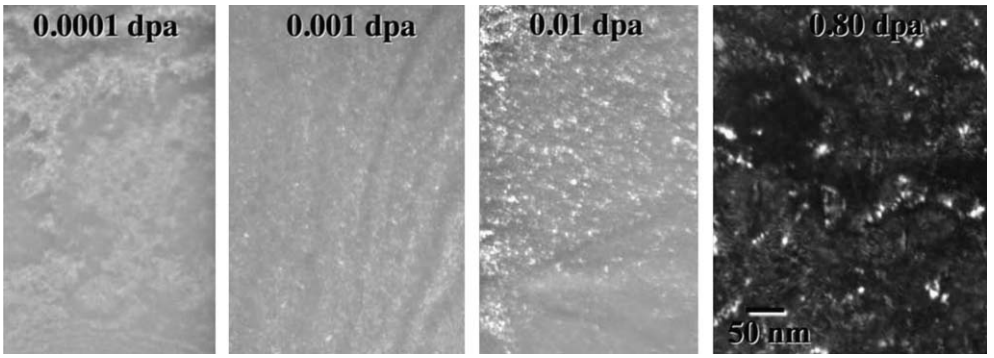

Fig. 1. Typical weak beam dark field microstructures of Fe irradiated in HFIR to doses of 0.0001–0.79 dpa. All micrographs were imaged using a zone axis of $B = 1\,1\,1$ and $(g, 4g)$, $g = 1\,\bar{1}\,0$ diffraction conditions except the 0.01 dpa micrograph that used $B = 1\,1\,0$ and $(g, 5g)$ $g = 002$.

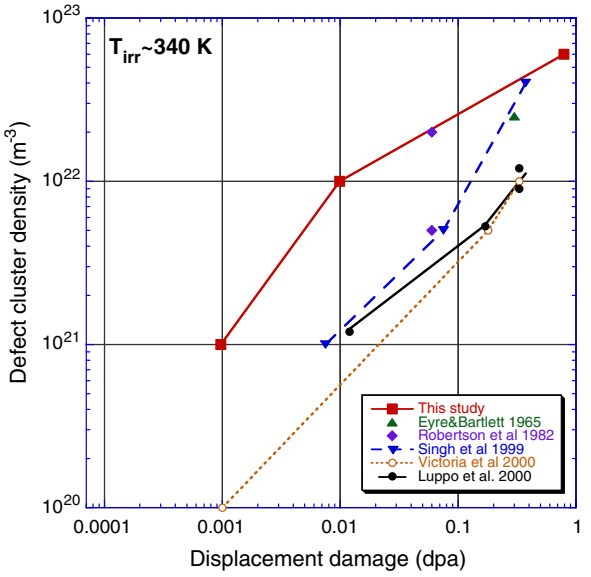

Fig. 2. Dose dependence of visible defect cluster density in neutron-irradiated Fe. Data from previous studies of fission neutron [8,9,15] and 600 MeV proton [7,16] irradiated Fe are shown for comparison.

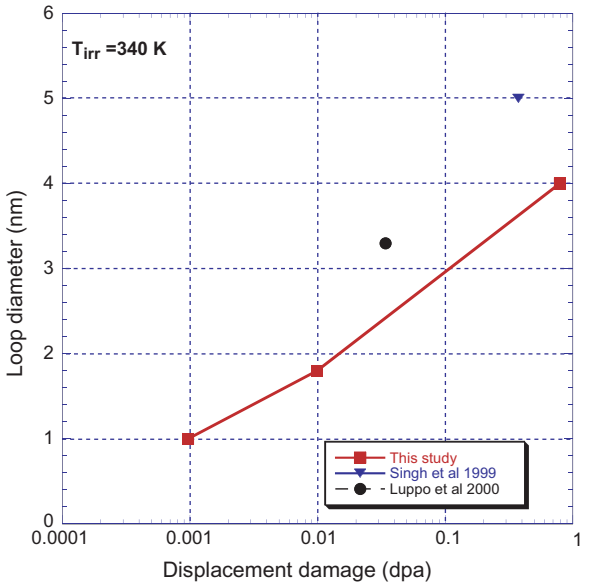

Fig. 3. Dose dependence of visible defect cluster size in neutron-irradiated Fe. Data from previous studies of fission neutron [8] and 600 MeV proton [7] irradiated Fe are shown for comparison.

planes. Approximately 15–20% of the loop rafts were aligned along {1 1 0} habit planes. The fraction of loop rafts aligned along {0 0 1} habit planes was <1%.

Fig. 5 shows the typical loop raft microstructures for a beam direction of ⟨0 0 1⟩. Loop rafts lying along {1 1 1} and {1 1 0} habit planes are visible for a diffraction vector of $g = 020$ in Fig. 5(a). Conversely, loop rafts lying along {0 0 1} habit planes were typically not observed for any diffraction conditions (<1% of total loop density). The loop raft on a given {1 1 1} or {1 1 0} habit plane typically consisted of a one-dimensional cluster of small loops aligned along a ⟨1 1 0⟩ direction within the habit plane, as opposed to being distributed as a two-dimensional platelet of defect clusters. For beam directions of ⟨0 0 1⟩, the habit planes for {1 1 0} and the projection of {1 1 1} habit planes coincide. Additional loop analyses using beam directions of ⟨1 1 0⟩ and ⟨1 1 1⟩ were used to distinguish between {1 1 0} and {1 1 1} habit planes. As shown in Fig. 5(b) and (c), when the diffraction vector is changed to $g = \langle 1\,1\,0\rangle$, the loop rafts lying on habit planes with their plane normal 90° to the diffraction vector are not visible. Similar diffraction contrast analysis performed for several different beam directions and diffraction vectors indicates that the loops within a given {1 1 1} raft exhibit contrast consistent with pure edge loops, i.e. Burgers vectors of $b = a/2\langle 1\,1\,1\rangle$. The loops within {1 1 0} rafts also exhibited contrast consistent with a Burgers vector of $b = a/2\langle 1\,1\,1\rangle$.

As shown in Fig. 6, individual small dislocation loops are resolvable within the rafts for a dose of 0.79 dpa. The number of loops comprising a raft packet ranged from 3 to 20. Most of the loop raft packets consisted of a single row of aligned loops. However, in about 5% of the loop rafts, two parallel sets of loops within a loop raft were observed. Although the individual loop habit planes within the rafts could not be accurately determined due to the small loop size, all of the loops within a given raft packet exhibited the same diffraction contrast during loop analysis performed with different diffraction vectors. Therefore, all loops within a given raft packet appear to have the same Burgers vector. Approximately 80% of the loops exhibit contrast consistent with pure edge $a/2\langle 1\,1\,1\rangle\{1\,1\,1\}$ loops. The loops located in rafts on {1 1 0·} planes exhibited diffraction contrast behavior consistent with $a/2\langle 1\,1\,1\rangle\{1\,1\,0\}$, suggesting that the loops in these rafts have not yet rotated on their glide plane to form the pure edge orientation.

As described elsewhere [14], positron annihilation spectroscopy analyses indicate that a three-dimensional vacancy cluster component is also

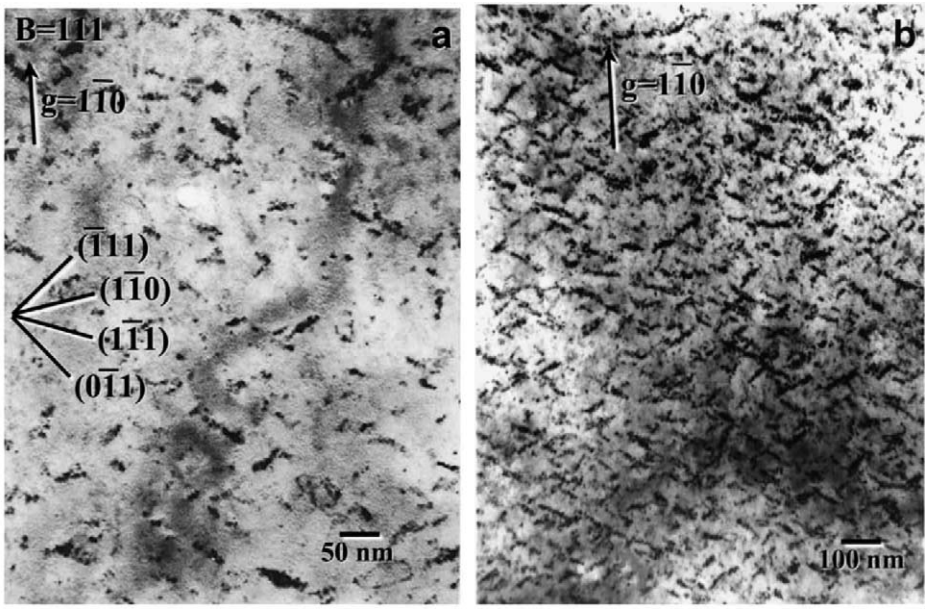

Fig. 4. Dislocation loop raft microstructure for a zone axis of $B = 111$ in (a) thin and (b) thick foil regions in Fe neutron irradiated to 0.79 dpa. Several projected loop habit planes are marked in (a).

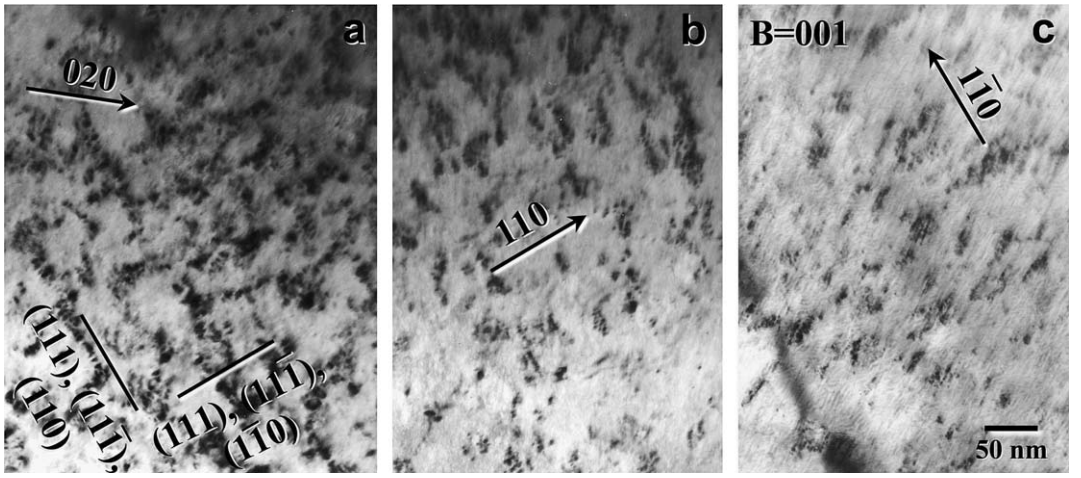

Fig. 5. Dislocation loop raft microstructures for $B = 001$ beam orientation in Fe following neutron irradiation to 0.79 dpa. The bright field diffraction vectors are indicated in (a)–(c) and the projected {110} and {111} habit planes are shown in (a).

present in the irradiated Fe specimens at all doses between 0.0001 and 0.79 dpa. The present TEM and previously reported positron [14] analyses were performed on the end tab regions of the same tensile specimens. The estimated cavity density from the positron analysis exceeded 1×10^{24} m^{-3} for doses above 0.001 dpa ($\sim 5 \times 10^{24}$ m^{-3} for 0.23 dpa), and the estimated cavity diameters ranged from 0.3 to 1.0 nm. Most of these cavities would be too small to be detectable by TEM, which has a cavity resolution limit near 1 nm. Small defects ~1 nm diameter with a density $>5 \times 10^{23}$ m^{-3} and exhibiting contrast consistent with small voids were observed during TEM examination of Fe irradiated to a dose of 0.79 dpa. Fig. 7 shows examples of these small cavities for kinematical underfocus and overfocus conditions. The cavities appear as white and dark spots for underfocused and overfocused imaging conditions, respectively. The cavities appear to be randomly distributed throughout the grain interior.

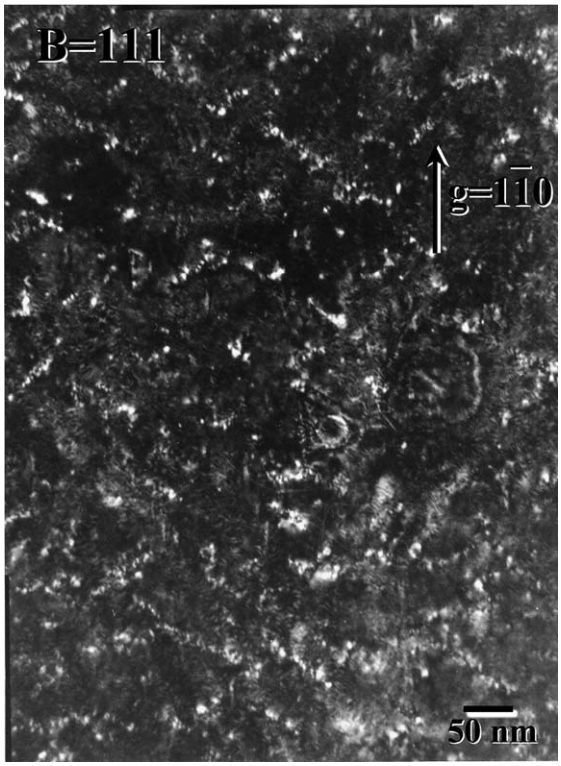

Fig. 6. Weak beam dark field $(-g,g)$, $g = 220$ microstructure of Fe neutron irradiated to 0.79 dpa showing individual loops that comprise dislocation rafts.

3.2. Tensile deformation microstructure

Table 1 summarizes the measured tensile properties of the unirradiated and irradiated Fe specimens. The unirradiated pure Fe specimens exhibited a yield strength of ~140 MPa and good work hardening capacity, with an ultimate tensile strength of ~215 MPa and a uniform elongation of nearly 30%. Tensile testing of neutron-irradiated Fe showed slight radiation hardening (~15 MPa) for a dose of 10^{-4} dpa, where defect clusters were not visible by TEM. Irradiation to a dose of 0.01 dpa reduced the uniform elongation to nearly zero, in contrast to the unirradiated uniform elongation of >25%. However, the total elongation remained relatively high with a value of ~17% following 0.01 dpa irradiation. Irradiation to 0.79 dpa caused substantial further hardening (upper yield strength of 355 MPa) and reduction in elongation, and a pronounced yield drop was evident. The total elongation in this case was ~5% (versus an unirradiated total elongation of >30%). The engineering stress–strain tensile curves [14] and additional tensile information [18] for the neutron-irradiated Fe specimens are given elsewhere.

The deformation microstructure of unirradiated Fe consisted predominantly of a cell structure with

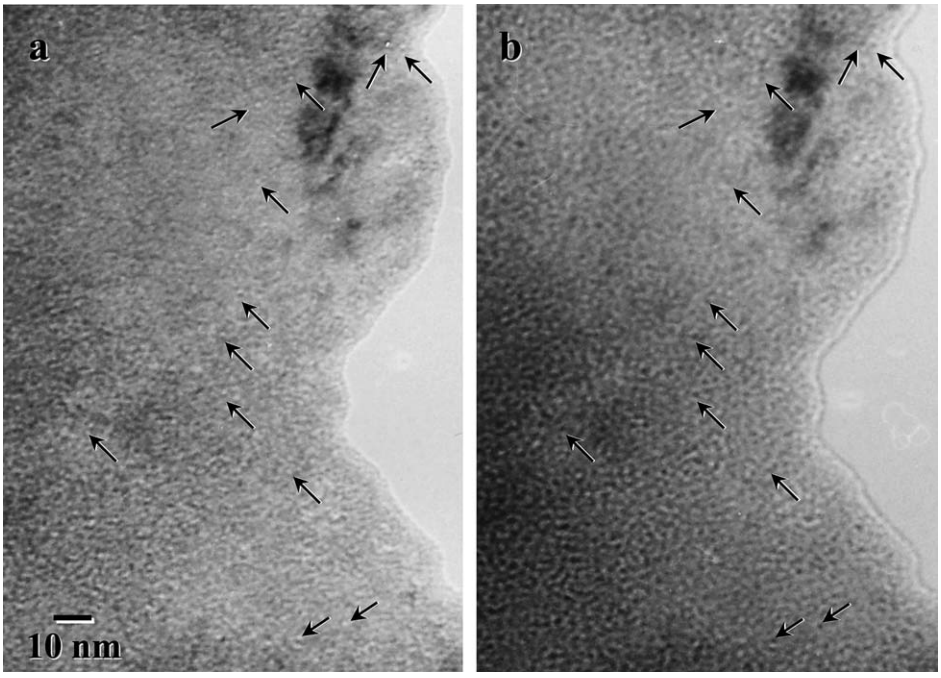

Fig. 7. Kinematic bright field images of cavities in Fe irradiated to 0.79 dpa at 70 °C for (a) underfocused and (b) overfocused conditions. The arrows point to several visible cavities.

Table 1
Summary of tensile properties of unirradiated and HFIR-irradiated Fe tested at 70 °C

Damage level (dpa)	0.05% Flow stress (MPa)	0.2% Yield stress (MPa)	Maximum stress (MPa)	Uniform elongation (%)	Total elongation (%)
0	138	138	230	28	30
0.00012	145	145	220	23	25
0.001	140	155	220	28	30
0.01	230	230	230	~0.05	17
0.79	360	360	360	~0.05	5.5

The maximum stress equals the ultimate tensile stress at low doses and the flow (0.05% plastic deformation) stress at high doses.

high dislocation density walls and lower dislocation density cell interiors. This cell structure appeared to be present in the post-irradiation deformation microstructure up to doses of ~0.2 dpa, although the examined thin regions of the 0.2 dpa specimens was rather limited. At doses of 0.4 dpa and higher, there was no evidence of cellular deformation structures during examination of extensive thin regions of the foils and the overall network dislocation density following deformation was comparable to that measured in irradiated non-deformed specimens.

Following irradiation to a dose of 0.79 dpa, much of the deformation microstructure in the uniform strain region was comparable to as-irradiated Fe. As shown in Fig. 8, loop rafts lying predominantly on {1 1 1} habit planes were still present following tensile deformation of Fe irradiated to 0.79 dpa. The distribution of habit planes of the loop rafts in the uniform strain region was similar to that observed in non-deformed specimens.

The most striking change in the microstructure of specimens tensile tested following irradiation at 0.4 and 0.79 dpa was the creation of cleared dislocation channels. The dislocation channels were associated with the 12 ⟨1 1 1⟩{1 1 0} slip systems and 12 ⟨1 1 1⟩{2 1 1} slip systems in BCC Fe. Fig. 9 shows the low-magnification microstructure of Fe irradiated to 0.4 dpa and then tensile tested. The orientation of the uniaxial stress applied during tensile testing is denoted by the large arrows in the figure. There was no evidence for any significant amount of deformation-induced network dislocations in the matrix regions between the cleared channels. It can be seen that most of the cleared dislocation channels are oriented near the maximum resolved shear stress position 45° from the applied uniaxial stress. In particular, the channels running diagonally from the lower left to the top right in Fig. 9 correspond to the $(1\bar{1}2)[\bar{1}11]$ and $(0\bar{1}1)[\bar{1}11]$ slip systems, which have the maximum resolved shear stress for {112} and {1 1 0} slip planes in this grain,

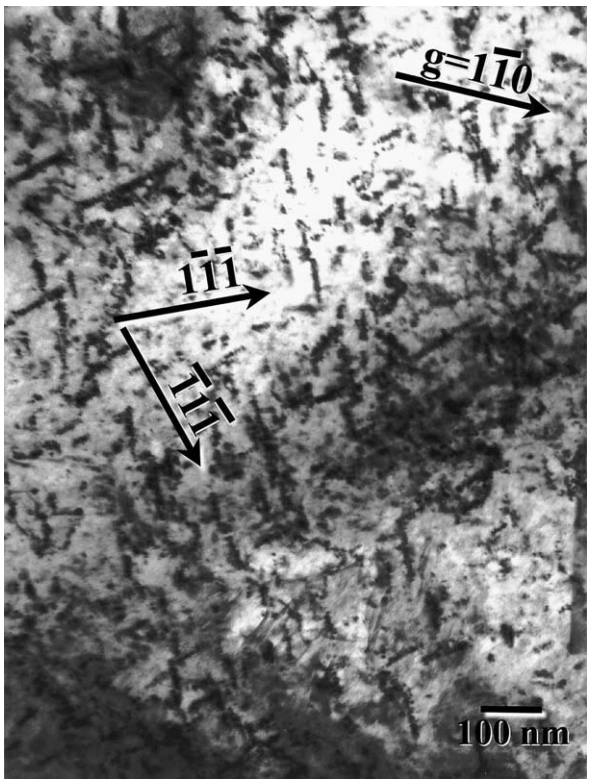

Fig. 8. Dislocation loop raft microstructure for [1 1 0] beam orientation in the uniform strain region of Fe neutron irradiated to 0.79 dpa and then tensile tested. The diffraction vector and loop raft habit planes are marked on the micrograph.

respectively. The horizontal dislocation channel corresponds to $(\bar{1}12)[1\bar{1}1]$ and $(21\bar{1})[1\bar{1}1]$ slip systems, both of which have a resolved shear stress that is only 40% of the maximum resolved shear stress. Since the horizontal dislocation channel appears to have formed prior to the diagonal channels (based on the large shear displacements of the horizontal channel where it intersects the diagonal channels), this suggests the dislocation source responsible for the horizontal channel formation may have been associated with a localized stress

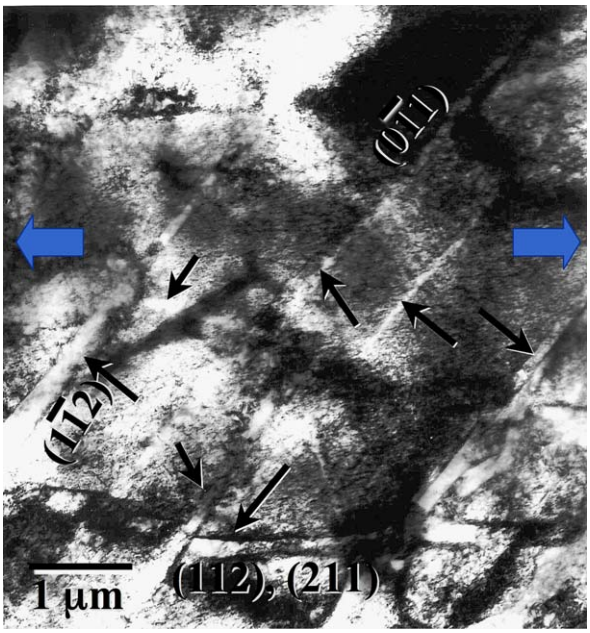

Fig. 9. General microstructure near the fracture surface of Fe irradiated to 0.4 dpa at 70 °C and then tensile tested. Several cleared channels are marked with small arrows. The large arrows show the direction of the applied uniaxial stress. The zone axis is near [1 1 1]. The slip plane traces for several dislocation channels are also labeled.

concentrator such as a grain boundary inclusion that caused the source to begin operation at relatively low applied stress.

Fig. 10 shows two examples of dislocation channels near the fracture surface of deformed Fe irradiated to a dose of 0.4 dpa. The left-hand micrograph clearly demonstrates the large amount of grain boundary deformation that occurs when a dislocation channel is transmitted through a grain boundary. The transmission of the dislocation channel created a localized ~0.2 μm shear deformation of the grain boundary over a lateral dimension of ~0.3 μm. Fig. 10(b) shows the intersection of two dislocation channels. The horizontal channel presumably formed earlier in the deformation process, and the channel running diagonally subsequently formed and produced a localized lattice displacement of ~0.15 μm. Dislocation channels in post-irradiation deformed specimens were observed for doses of 0.1 dpa and higher. The dislocation channels following irradiation to 0.1 dpa were primarily observed near grain boundaries for a specimen taken near the fracture surface.

The dislocation channels were generally, but not always, fully cleared of defects. At doses of 0.4 and 0.79 dpa, residual dislocations and debris from partially annihilated defect clusters were occasionally observed within the cleared channel. Localized dislocation debris was often observed within dislocation channels in the vicinity of intersections with grain boundaries and other channels (e.g., Fig. 10). The average dislocation channel width ranged from 100 to 200 nm for specimens irradiated to 0.79 dpa.

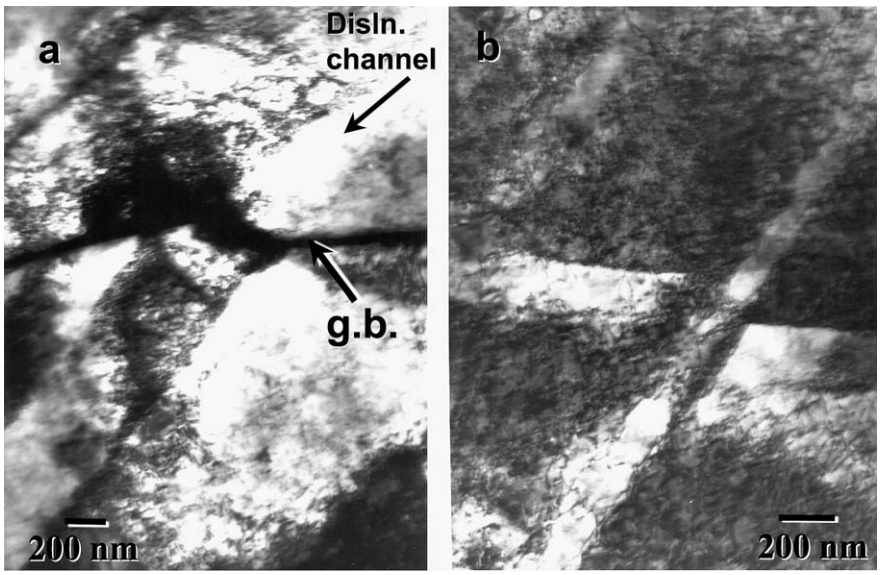

Fig. 10. Dislocation channels near the fracture surface of Fe irradiated to a dose of 0.4 dpa at 70 °C and tensile tested: (a) dislocation channel impinging on a grain boundary (g.b.) and (b) intersection of two channels.

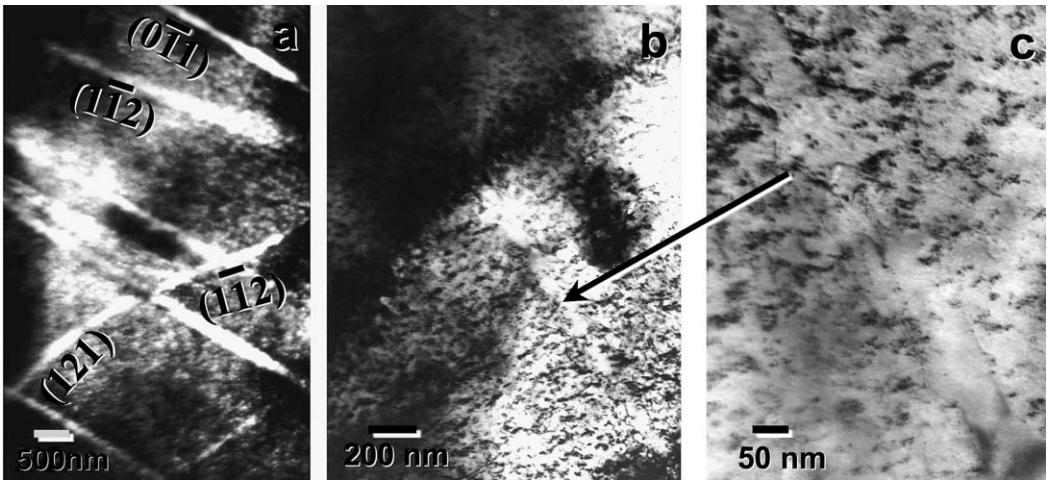

Fig. 11. Deformation microstructure of 0.79 dpa-irradiated iron for regions located (a) near the fracture surface and (b), (c) in the uniform strain region. The slip plane traces for several dislocation channels are labeled in (a).

The corresponding average spacing between dislocation channels varied from ~1.5 to ≫5 μm depending on crystal orientation (localized resolved shear stress) and whether the observation was made in the uniform strain region or near the fracture surface. As shown in Fig. 9, the spacing between channels was smallest for slip plane systems oriented ~45° from the tensile axis, i.e. on slip plane systems with the largest resolved shear stress.

The number of cleared dislocation channels was considerably higher in TEM specimens taken near the fracture surface compared to the uniform strain region in the tensile gage section. Fig. 11 compares the deformation microstructure of Fe irradiated to 0.79 dpa for regions near the fracture surface (<0.5 mm from the fracture surface) and in the uniformly strained gage region approximately 3 mm from the fracture surface. The spacing between dislocation channels was more than one order of magnitude larger in the uniform strain region compared to the fracture surface region. The average width of the cleared channels was comparable for the two regions. Therefore, the higher plastic strain associated with the necked region next to the fracture surface produced a higher density of cleared dislocation channels compared to the uniform strain region where the engineering elongation was only ~0.1%. This is presumably due to the activation of a larger number of dislocation sources in the necked region due to the multiaxial stress state. Cleared channels were observed on both {1 1 2} and {1 1 0} slip planes in the necked region.

Another significant difference between dislocation channels in the uniform strain versus necked regions is that visible bending or bifurcation of dislocation channels was observed for channels that formed near the fracture surface. Fig. 12 shows two examples of bending in dislocation channels obtained from locations near the fracture surface following tensile deformation of Fe irradiated to 0.79 dpa. Cleared dislocation channels lying on a specific crystallographic plane can be seen bending to other slip plane systems. For example, most of the channels in Fig. 12(b) have $(1\bar{1}0)$ slip planes but one of the channels appears to bend to a $(10\bar{1})$ slip plane. Possible causes of this bending of dislocation channels will be discussed in Section 4.2.

4. Discussion

4.1. As-irradiated microstructure

As summarized in Fig. 13, the dislocation loop density in irradiated Fe visible by TEM is about two orders of magnitude smaller than the cavity density determined from positron annihilation spectroscopy (PAS) [14] for all doses up to ~0.2 dpa following neutron irradiation at 50–70 °C. Transmission electron microscopy cannot detect isolated monovacancies or self-interstitial atoms, and in general can only detect defect clusters larger than ~0.5 to 1.0 nm depending on the degree of strain with the surrounding lattice. Due to the small size of the

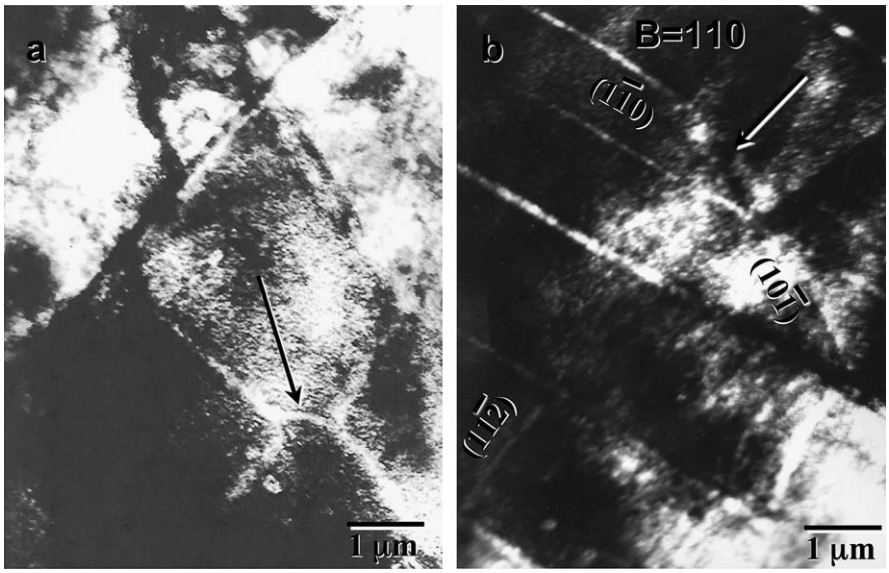

Fig. 12. Bending of dislocation channels in 0.79 dpa irradiated Fe as observed in regions near the fracture surface. The arrows mark examples of bent channels. The slip plane traces for several dislocation channels are labeled in (b).

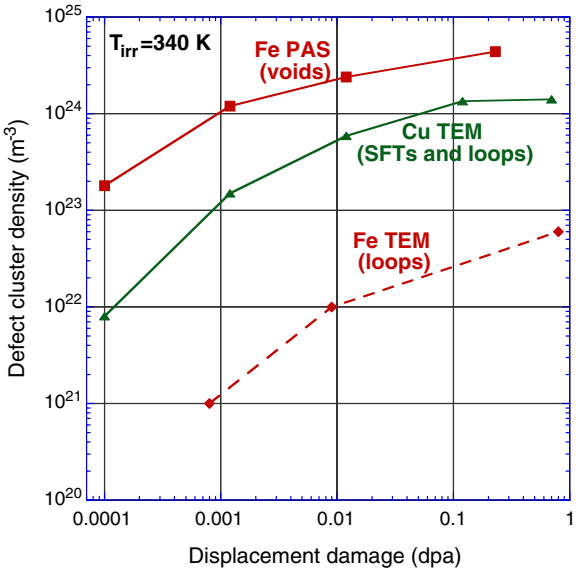

Fig. 13. Comparison of dose dependence of defect cluster densities in Fe and Cu following fission neutron irradiation at ~70 °C, replotted from Ref. [14].

dislocation loops in the present study, their nature (interstitial versus vacancy) was not determined. Previous work has found nearly all analyzed loops in Fe to be interstitial-type following neutron irradiation at 50–200 °C [5,9,12,19]. The PAS data, obtained on the end tab regions of the same irradiated Fe tensile specimens as the present TEM study, suggest there is a significant population of submicroscopic three-dimensional cavities with an average diameter near 0.5 nm [14]. The PAS-analyzed density of the nano-cavities ranged from $\sim 1 \times 10^{23}$ m^{-3} at 0.0001 dpa to 4.5×10^{24} m^{-3} at 0.23 dpa. Small cavities with a maximum diameter of ~1.5 nm were observed by TEM in the Fe specimens irradiated to a dose of 0.79 dpa (Fig. 8), in qualitative agreement with the PAS analysis. However, most of the cavities detected by PAS (average diameter of ~0.5 nm) were below the TEM cavity resolution limit (~1.0 nm).

It is noteworthy that such a high density of cavities was observed in irradiated Fe at this low homologous irradiation temperature of 0.19 T_M, where T_M is the melting temperature. The cavity swelling determined from PAS analysis ranged from 4×10^{-4}% at 0.0001 dpa to 5×10^{-2}% at 0.23 dpa [14]. This increase in cavity swelling with increasing dose is due to a combination of cavity growth and increased cavity nucleation [14]. Vacancies become mobile in Fe at temperatures near −20 °C (recovery Stage III) [20,21]. The irradiation temperature in the present study is below the recovery Stage IV temperature in Fe (150–325 °C), which has recently been attributed to dissociation of small sessile vacancy clusters consisting of five or more vacancies [20]. This suggests that the cavity swelling in these neutron-irradiated Fe specimens is predominantly associated with migration and coalescence of

monovacancies and small mobile vacancy clusters (containing four or fewer vacancies), either by correlated events within a single displacement cascade or via uncorrelated interactions with adjoining displacement cascades. The presence of void swelling at this relatively low homologous temperature in Fe (0.19 T_M) has also been reported to occur for several other irradiated BCC metals [22] and is in stark contrast to the void swelling behavior in neutron-irradiated FCC metals that generally requires irradiation at temperatures above recovery stage V (dissolution of large sessile vacancy clusters), corresponding to ~0.3 T_M [22–24].

The defect cluster density and size data summarized in Figs. 2 and 3 contain several important observations regarding interstitial cluster formation in pure iron irradiated with neutrons near room temperature. First, there is a threshold dose (~0.001 dpa) below which defect clusters cannot be seen by current transmission electron microscopes. Second, the visible defect cluster size increases monotonically with increasing dose at least up to 0.79 dpa. Finally, the visible defect cluster density increases with increasing dose and does not exhibit signs of reaching a saturation density for doses up to 0.79 dpa. These findings are discussed in more detail below.

The present observations regarding dislocation loop formation are in general agreement with published literature on neutron-irradiated Fe. Previous work on Fe irradiated with neutrons near room temperature was limited to a maximum dose of ~0.3 dpa [5,7–9,15,16,25]. At low doses, defect clusters are not observable by TEM in neutron-irradiated Fe [5,9–11,25]. The threshold fluence for defect cluster visibility was $\sim 4.5 \times 10^{22}$ n/m^2, $E > 1$ MeV (0.001 dpa) in the present study, whereas earlier work [5,9] did not observe clusters until fluences above $\sim 7 \times 10^{22}$ n/m^2 ($E > 1$ MeV). This small difference in the threshold dose for resolvable defect clusters may be due to improvements in electron microscope resolution as well as possible differences in impurity levels in the 'pure' Fe specimens. In the present study, the measured loop density was higher (Fig. 2) and the average loop size was smaller (Fig. 3) compared to previous work. Once again, this may be due to differences in solute impurities for the different 'pure' Fe specimens used in the studies, and may also be due to improvements in electron microscope resolution (the poorer resolution limits for earlier TEM studies compared to current electron microscopes would decrease the apparent density and increase the measured size compared to the actual values). Work by Okada et al. [11] has shown that the threshold dose for observable defect clusters in neutron-irradiated Fe decreases with increasing irradiation temperature between 200 and 300 °C.

The lack of visible defect clusters at a dose of 0.0001 dpa indicates that large (>1 nm) sessile defect clusters are not produced directly in displacement cascades during fission neutron irradiation of Fe. Previous TEM studies on Fe irradiated with 14 MeV neutrons indicates that visible sessile defect clusters are not produced at room temperature even for high primary knock-on atom energies [25,26]. Molecular dynamics simulations of irradiated Fe have found significant amounts of defect cluster formation occur directly in displacement cascades within ~0.1 ns time scales [27–29]. However, the size of the defect clusters in these simulations is generally below the visibility limit for TEM, and many of the created defect clusters are highly glissile at room temperature based on molecular dynamics [27–30] and ab initio [20] simulations. During prolonged irradiation, these glissile clusters could interact to form larger sessile loops that would be visible by TEM. Conversely, molecular dynamics simulations of 50 keV cascades in Fe by Soneda et al. [31] suggest that large (~2nm diameter) vacancy and interstitial loops could be directly created in about 1% of displacement cascades, which corresponds to a visible defect cluster density of $\sim 1 \times 10^{20}$ m^{-3} for a damage level of 10^{-4} dpa. For the imaging conditions used in the present investigation, visible defect cluster densities as low as $\sim 1 \times 10^{19}$ m^{-3} would have been detectable. Therefore, although we cannot experimentally exclude the possibility that some large (~1 to 2 nm) defect clusters ($<10^{19}$ m^{-3}) are produced directly in displacement cascades of fission neutron-irradiated Fe, the production of TEM-visible defect clusters could occur in at most 0.1% of the displacement cascades (i.e., at least one order of magnitude smaller than suggested by Soneda et al.).

The defect cluster evolution in Fe is different from the behavior of medium atomic number face centered cubic metals such as Ni and Cu where defect clusters visible by TEM are created even at doses below 0.0001 dpa [24,26,32–34], i.e., at doses where formation by point defect migration and growth from a variety of displacement cascade events is unlikely. As shown in Fig. 13, the TEM-visible defect cluster density in copper irradiated

near room temperature approaches a constant value due to cascade overlap effects for doses above ~0.1 dpa [24]. The defect cluster density detected by TEM in Cu (predominantly SFTs) is significantly less than the cavity density in Fe determined by PAS, but is significantly above the TEM-visible defect cluster density in Fe. The visible defect clusters in the FCC metals Cu and Ni at low doses are >90% vacancy-type clusters (stacking fault tetrahedra) [35], whereas the TEM-visible defect clusters in Fe are considered to be interstitial dislocation loops based on previous loop analyses [5,9,12,19] and due to the high concentration of vacancies in the nano-cavities detected by PAS. Molecular dynamics simulations have found large sessile defect clusters (predominantly vacancy-type) are created within the displacement cascades in FCC metals such as Cu [27,28,36,37]. Similarly, TEM studies of ion-beam-induced dislocation loop formation have found that the efficiency of direct production of vacancy loops from 100 keV self-ions at room temperature is approximately two orders of magnitude lower for Fe compared to Cu and Ni [38]. These observations suggest that the formation of visible defect clusters in fission neutron-irradiated Fe occurs via point defect nucleation and growth, as opposed to direct in-cascade formation of visible (>1 nm diameter) defect clusters that occurs in Cu and Ni.

The number of surviving vacancies and self interstitial atoms contained in nano-cavities and dislocation loops can be calculated from the PAS [14] and TEM data, respectively. The quantitative difference between the measured residual vacancy and interstitial concentrations in cavities and loops, respectively suggests that many of the self-interstitial atoms initially created by irradiation are either in submicroscopic defect clusters or have been annihilated by long-range migration to permanent defect sinks such as dislocations or grain boundaries. At low doses of 0.001–0.01 dpa, the cumulative concentration of interstitials contained in TEM-visible loops was more than one order of magnitude lower than the sum of vacancies in nano-cavities. For example, the total measured surviving interstitial and vacancy concentrations after 0.01 dpa were 6×10^{-6} and 2×10^{-4} atom fractions, respectively. After irradiation to 0.4 dpa, the number of interstitials contained in visible loops (2×10^{-4}) was only a factor of three lower than the number of vacancies in cavities (6×10^{-4}). The low absolute magnitude of the measured residual defect concentrations of both vacancies and interstitials (in isolated or clustered form) compared to the dpa value suggests there has been significant recombination of interstitial- and vacancy-type defects during the irradiation even at low doses of ~0.0001 to 0.001 dpa. Even at the lowest investigated dose (0.0001 dpa), only about 4% of the created vacancy population based on the calculated displacement damage was detected by PAS as residual damage in the form of small cavities [14]. The calculated point defect sink strength of the cavities based on the PAS analysis is $\sim5\times10^{14}\,m^{-2}$ at a dose of 0.0001 dpa and is $\sim3\times10^{15}\,m^{-2}$ at 0.001 dpa. Such high cavity sink strengths would cause significant annihilation of glissile interstitial-type defects and hence lead to a substantial reduction in the residual clustered vacancy and interstitial concentrations compared to the dpa value.

Dislocation loop analyses of neutron-irradiated Fe have been limited to relatively large loops (diameters >10 nm) [5,9,12]. These previous studies reported near-edge loop orientations with $b = a\langle001\rangle$ and $a/2\langle111\rangle$ (i.e., habit planes of {001} and {111}, respectively). The $a/2\langle111\rangle\{111\}$ loops were the most common loop configuration in previous studies. In the present study, most of the ~4 nm defect clusters in the 0.79 dpa Fe specimen exhibited diffraction contrast consistent with $a/2\langle111\rangle\{111\}$ loops, and about 15–20% of the defect clusters appeared to be $a/2\langle111\rangle\{110\}$ loops. Less than 1% of the defect clusters in the present study exhibited contrast consistent with $a/\langle001\rangle\{001\}$ loops. Molecular dynamics simulations of fission neutron-irradiated Fe have reported that many of the interstitial defects created directly in the displacement cascade are in the form of small (typically containing up to ~30 interstitials) clusters with $a/2\langle111\rangle$ Burgers vectors on {110} habit planes [27–31]. The simulations indicate these $a/2\langle111\rangle\{110\}$ clusters are highly glissile at room temperature. The presence of $a/2\langle111\rangle$ loops on both {111} and {110} planes may be rationalized as evidence for a loop evolution process where visible $a/2\langle111\rangle\{110\}$ perfect loops are created from coalescence of smaller $a/2\langle111\rangle\{110\}$ glissile clusters, and these loops subsequently rotate on their glide cylinder to form edge-type $a/2\langle111\rangle\{111\}$ loops.

The relatively high fraction (~80%) of near-edge $a/2\langle111\rangle\{111\}$ loops in Fe irradiated near 70 °C in the present study agrees with results obtained on other irradiated BCC metals such as molybde-

num [39–41], and for vanadium irradiated at temperatures above 300 °C [42]. Conversely, previous studies on neutron-irradiated Fe have found that $a/\langle 001\rangle\{001\}$ loops become increasingly prevalent with increasing irradiation temperature: Most loops in Fe neutron-irradiated above 250 °C are reported to be $a\langle 001\rangle\{001\}$ loops [11–13,43]. The existence of some loops with $a/2\langle 111\rangle\{110\}$ and $a/\langle 001\rangle\{001\}$ orientations is qualitatively consistent with the Eyre–Bullough mechanism of transformation of small faulted $a/2\langle 110\rangle\{110\}$ loops by shear mechanisms [44]. The shear dislocation energy associated with creation of $a\langle 001\rangle$ loops is energetically unfavorable compared to $a/2\langle 111\rangle$ and therefore $a/2\langle 111\rangle$ loops would be predicted to preferentially form, especially at low temperatures. At high temperatures, thermal energy could reduce the importance of differences in dislocation loop elastic energies and lead to increasing numbers of $a/\langle 001\rangle\{001\}$ loops. However, the validity of the Eyre–Bullough mechanism is uncertain since molecular dynamics simulations of Fe find that $a/2\langle 111\rangle\{110\}$ perfect loops are created by displacement cascades instead of $a/2\langle 110\rangle\{110\}$ faulted loops [27–31]. Based on molecular dynamics simulations, Marian, Wirth and Perlado proposed that interstitial clusters in Fe initially nucleate as $a/2\langle 111\rangle\{110\}$ loops and that $a\langle 001\rangle$ loops can be formed by interactions between impinging $a/2\langle 111\rangle$ loops [45]. Due to increased atomic mobility at high temperatures, the fraction of $a\langle 001\rangle$ loops in Fe might also be expected to increase with increasing irradiation temperature for the Marian et al. mechanism. Their mechanism for the formation of $a\langle 001\rangle$ loops requires transformation of an intermediate metastable $a/2\langle 110\rangle$ loop with an activation barrier on the order of 1.0 eV [45]. This activation barrier would be prohibitively high for irradiations at temperatures below ~100 °C and therefore the Marian et al. mechanism is consistent with the present TEM observations of a practical absence of $a\langle 001\rangle$ loops following neutron irradiation at 50–70 °C, and previously reported observations [11–13,43] of a high fraction of $a\langle 001\rangle$ loops at temperatures above 250 °C.

The present study appears to be the first reported observation of loop rafts in iron following neutron irradiation near room temperature. A previous study of neutron-irradiated Fe reported the presence of three-dimensional clusters of $a\langle 001\rangle$ loops at intermediate temperatures of 275 and 300 °C following irradiation to ~1 dpa [12]. These loop clusters were not observed at temperatures between 182 and 250 °C, which were the lowest temperatures investigated in ref. [12]. In the present study, irradiation to 0.79 dpa at 70 °C resulted in well-developed loop rafts (Figs. 4–6) aligned along $\langle 110\rangle$ directions primarily on $\{111\}$ habit planes. Partial development of loop rafts was detectable in specimens irradiated to 0.4 dpa. All of the loops for a given raft appeared to have the same Burgers vector (predominantly $a/2\langle 111\rangle$). These loop raft observations for Fe are consistent with the behavior seen in irradiated Mo [17,39,46], TZM molybdenum alloy [39,47–49], and tungsten [50], where loop rafts along $\langle 110\rangle$ directions on $\{111\}$ habit planes were observed following irradiation to doses above ~0.1 dpa. There was a tendency for raft formation in TZM to be most pronounced for intermediate temperatures near ~400 °C.

4.2. Tensile deformation microstructure

The threshold dose for well-developed dislocation channels in pure Fe neutron irradiated and tensile tested at ~70 °C lies near 0.4 dpa based on the present investigation (e.g., Fig. 9). A mixture of dislocation cell formation and dislocation channels adjacent to grain boundaries was observed in tensile-tested Fe irradiated to 0.1 dpa (DR-3 reactor), and dislocation cell formation was observed in Fe irradiated to 0.3 dpa in BR-2. However, the limited thin area in these two specimens precluded a comprehensive quantitative study of the relative proportion of cell formation versus dislocation channeling. Previous work by Singh et al. reported well-developed dislocation channels following tensile testing of Fe irradiated to 0.4 dpa, and primarily homogeneously distributed dislocations mixed with a few localized deformation bands following irradiation at 0.075 dpa but no indication of dislocation cell structure [8]. Earlier work found evidence for dislocation channeling in tensile tested Fe that was neutron irradiated to fluences $>1\times10^{23}$ n/m^2, which corresponds to a damage level of only ~0.01 dpa [51]. Slip band coarsening was also observed for neutron fluences as low as 5×10^{22} n/m^2 [51]. Pinning of dislocations by submicroscopic defect clusters was also detected following deformation of Fe irradiated to neutron fluences ($E>1$ MeV) of 5×10^{22} and 5×10^{23} n/m^2 [5,51], along with evidence for restricted (localized) dislocation motion [52] which may be a precursor to full-fledged dislocation channeling. The average cleared

channel width observed in specimens irradiated to 0.4–0.79 dpa in the present study (100–200 nm) is similar to a previous observation by Eyre [51], but is slightly larger than the 60–100 nm width reported by Luppo et al. [7] for Fe irradiated to a dose of 0.3 dpa.

The highly localized stresses associated with dislocation channeling (cf. Fig. 10) clearly mandate the use of well-engineered materials for structural applications in order to minimize the probability of crack formation at grain boundaries or other lattice interfaces. Evidence for enhanced intergranular cracking in irradiated pure Fe following room temperature tensile testing has been reported for doses above 10^{-3} dpa and was attributed to dislocation channeling [6].

It is worth noting the differences in the deformation structures in the uniform strain and necked regions of irradiated Fe tensile specimens (Fig. 11). Although cleared dislocation channels were observed in both regions of Fe specimens irradiated to doses of 0.4–0.79 dpa, the spacing between dislocation channels was considerably smaller for the necked region of the tensile specimen ($\sim$1.5 μm spacing) compared to a spacing $\gg$5 μm in the uniform strain region. This is attributed to activation by multiaxial stresses and/or grain rotation of additional dislocation sources on slip systems that were not favorably oriented for operation by the initially imposed uniaxial tension stress state. The locally higher tensile stresses created in the necked region may also activate additional dislocation sources that were not operational at lower stresses.

Considerable twisting and bifurcation of dislocation channels was observed in the necked regions of deformed irradiated specimens (Fig. 12). Bending of dislocation channels has been previously observed in other irradiated BCC metals such as pure and alloyed vanadium [42,53,54]. This may be attributed in part to the presence of numerous available slip systems in BCC metals (12 each on {1 1 1} and {2 1 1} slip planes), and due to presence of a multiaxial stress state during necking versus nearly pure uniaxial stress in the uniform strain region. Multiaxial strains imposed by constraint considerations with adjacent grains during intense deformation may also be an important factor. An increased frequency of bent dislocation channels compared to uniaxial tensile strained specimens was observed in pure vanadium neutron irradiated to 0.7 dpa near room temperature and subsequently deformed at room temperature by a ball indenter that introduced a high multiaxial stress component compared to uniaxial tensile tests [55].

5. Conclusions

The defect cluster size and density detectable by TEM in pure Fe increases steadily with increasing dose for neutron irradiation near room temperature to doses of 0.001–0.79 dpa. Conversely, defect clusters are not visible in Fe irradiated to a dose of 0.0001 dpa. Therefore, the efficiency of direct in-cascade production of visible defect clusters in fission neutron irradiated iron is <0.1%. These observations suggest that defect cluster formation in fission neutron-irradiated Fe occurs via point defect nucleation and growth, as opposed to in-cascade formation of visible (>1 nm diameter) sessile vacancy clusters that occurs in medium atomic number face centered cubic metals such as Ni and Cu.

A high density of small three-dimensional vacancy clusters is produced by the 70 °C neutron irradiation but is not visible by TEM. Only the largest cavities (>1 nm) at a dose of 0.79 dpa were detected using TEM. Differences in the cumulative total of surviving vacancies and interstitials in clusters detected by positron annihilation spectroscopy and TEM suggest that many of the interstitial defects (point defects or clusters) are mobile near room temperature and are annihilated following migration to permanent sinks such as dislocations or grain boundaries. In addition, the low concentration of residual vacancies and interstitials compared to the dpa value indicates that most of the initially created defects are annihilated by recombination events following short- or long-range diffusion.

The formation of local 'rafts' of dislocation loops occurs for doses above 0.3 dpa. The raft formation occurs predominantly on {1 1 1} habit planes and all loops associated with a given raft appear to have similar Burgers vectors. Most of the loops have diffraction contrast consistent with near-edge $a/2\langle 1\,1\,1\rangle\{1\,1\,1\}$ loops, with a smaller fraction of $a/2\langle 1\,1\,1\rangle\{1\,1\,0\}$ loops. Very few $a\langle 0\,0\,1\rangle\{0\,0\,1\}$ loops were detected for the present irradiation conditions. These observations are qualitatively consistent with the Eyre–Bullough and Marian et al. loop evolution mechanisms.

Neutron irradiation of pure Fe to doses above 0.1 dpa near room temperature resulted in very low uniform elongation in uniaxial tensile tests. Dislocation channels that are essentially cleared of defect clusters and dislocation remnants are

observed in the deformed regions of irradiated Fe at doses above 0.1 dpa, and dislocation channels become the predominant deformation mode at damage levels of 0.4 dpa or higher. This corresponds to the critical dose for prompt plastic instability during tensile testing. Dislocation cell structures are predominantly observed following deformation of Fe irradiated to lower damage levels.

The presence of a multiaxial stress state (i.e., near the necked region of tensile specimens) significantly increases the number density of dislocation channels in irradiated Fe. This is attributed to activation of additional dislocation sources on slip systems not favorably oriented for activation by uniaxial tension. The presence of a multiaxial stress state also enhances the bending of dislocation channels among the numerous available slip systems in BCC metals.

Acknowledgements

The authors thank K. Farrell and T.S. Byun for irradiation of the Fe specimens in HFIR, and Gitte Christiansen for preparation of the TEM foils. The neutron irradiation of the specimens was supported by the Division of Materials Science in the Office of Basic Energy Sciences, US Department of Energy. This research was sponsored by the Office of Fusion Energy, US Department of Energy, under contract number DE-AC05-00OR22725 with UT-Battelle, LLC, and by the European Fusion Technology Programme.

References

[1] R.L. Klueh, D.R. Harries, High-Chromium Ferritic and Martensitic Steels for Nuclear Applications, American Society for Testing and Materials, West Conshohocken, PA, 2001.
[2] L.K. Mansur, A.F. Rowcliffe, R.K. Nanstad, S.J. Zinkle, W.R. Corwin, R.E. Stoller, J. Nucl. Mater. 329–333 (2004) 166.
[3] R.L. Klueh, Current Opinions Sol. State Mater. Sci. 8 (2004) 239.
[4] R.L. Klueh, Intern. Mater. Rev. 50 (5) (2005) 287.
[5] E.A. Little, Intern. Metals Rev. 21 (1976) 25.
[6] Y. Chen, P. Spaetig, M. Victoria, J. Nucl. Mater. 271&272 (1999) 128.
[7] M.I. Luppo, C. Bailat, R. Schäublin, M. Victoria, J. Nucl. Mater. 283–287 (2000) 483.
[8] B.N. Singh, A. Horsewell, P. Toft, J. Nucl. Mater. 271&272 (1999) 97.
[9] I.M. Robertson, M.L. Jenkins, C.A. English, J. Nucl. Mater. 108&109 (1982) 209.
[10] J.S. Bryner, Acta Metall. 14 (1966) 323.
[11] A. Okada, T. Yasujima, T. Yoshiie, I. Ishida, M. Kiritani, J. Nucl. Mater. 179–181 (1991) 1083.
[12] L.L. Horton, J. Bentley, K. Farrell, J. Nucl. Mater. 108&109 (1982) 222.
[13] A.C. Nicol, M.L. Jenkins, M.A. Kirk, in: G.E. Lucas et al. (Eds.), Microstructural Processes in Irradiated Materials–2000, MRS Symposium Proceedings, vol. 650, Materials Research Society, Warrendale, PA, 2001, p. R1.3.1.
[14] M. Eldrup, B.N. Singh, S.J. Zinkle, T.S. Byun, K. Farrell, J. Nucl. Mater. 307–311 (2002) 912.
[15] B.L. Eyre, A.F. Bartlett, Philos. Mag. 12 (1965) 261.
[16] M. Victoria et al., J. Nucl. Mater. 276 (2000) 114.
[17] J.L. Brimhall, B. Mastel, Radiat. Eff. 3 (1970) 203.
[18] T.S. Byun, K. Farrell, J. Nucl. Mater. 326 (2004) 86.
[19] M. Horiki, T. Yoshiie, M. Iseki, M. Kiritani, J. Nucl. Mater. 271&272 (1999) 256.
[20] C.C. Fu, J. Dalla Torre, F. Willaime, J.L. Bocquet, A. Barbu, Nature Mater. 4 (2005) 68.
[21] H. Schultz, Mater. Sci. Eng. A 141 (1991) 149.
[22] B.N. Singh, J.H. Evans, J. Nucl. Mater. 226 (1995) 277.
[23] S.I. Golubov, B.N. Singh, H. Trinkaus, J. Nucl. Mater. 276 (2000) 78.
[24] B.N. Singh, S.J. Zinkle, J. Nucl. Mater. 206 (1993) 212.
[25] T. Yoshiie, Y. Satoh, H. Taoka, S. Kojima, M. Kiritani, J. Nucl. Mater. 155–157 (1988) 1098.
[26] H. Fukushima, Y. Shimomura, J. Nucl. Mater. 205 (1993) 59.
[27] Y.N. Osetsky, D.J. Bacon, A. Serra, Philos. Mag. A 79 (1999) 273.
[28] Y.N. Osetsky, D.J. Bacon, A. Serra, B.N. Singh, S.I. Golubov, J. Nucl. Mater. 276 (2000) 65.
[29] R.E. Stoller, J. Nucl. Mater. 276 (2000) 22.
[30] J. Marian et al., Phys. Rev. B 65 (2002) 144102.
[31] N. Soneda, S. Ishino, T. Diaz de la Rubia, Philos. Mag. Lett. 81 (2001) 649.
[32] M. Kiritani, J. Nucl. Mater. 137 (1986) 261.
[33] S.J. Zinkle, J. Nucl. Mater. 150 (1987) 140.
[34] S.J. Zinkle, Radiat. Eff. Def. Solids 148 (1999) 447.
[35] S.J. Zinkle, L.L. Snead, J. Nucl. Mater. 225 (1995) 132.
[36] K. Nordlund, F. Gao, Appl. Phys. Lett. 74 (1999) 2720.
[37] Y.N. Osetsky, D.J. Bacon, Nucl. Instrum. and Meth. B 180 (2001) 85.
[38] M.A. Kirk, I.M. Robertson, M.L. Jenkins, C.A. English, T.J. Black, J.S. Vetrano, J. Nucl. Mater. 149 (1987) 21.
[39] J. Bentley, B.L. Eyre, M.H. Loretto, in: M.T. Robinson, F.W. YoungJr. (Eds.), Fundamental Aspects of Radiation Damage in Metals, CONF-751006-P2, vol. II, National Tech. Inform. Service, Springfield, VA, 1975, p. 925.
[40] C.A. English, J. Nucl. Mater. 108&109 (1982) 104.
[41] B.L. Eyre, J. Phys. F 3 (1973) 422.
[42] P.M. Rice, S.J. Zinkle, J. Nucl. Mater. 258–263 (1998) 1414.
[43] R. Bullough, R.C. Perrin, Proc. Royal Soc. A 305 (1968) 541.
[44] B.L. Eyre, R. Bullough, Philos. Mag. 12 (1965) 31.
[45] J. Marian, B.D. Wirth, J.M. Perlado, Phys. Rev. Lett. 88 (2002) 255507.
[46] B.N. Singh, J.H. Evans, A. Horsewell, P. Toft, G.V. Müller, J. Nucl. Mater. 258–263 (1998) 865.
[47] J. Bentley, B.L. Eyre, M.H. Loretto, in: J.S. Watson, F.W. Wiffen (Eds.), Radiation Effects and Tritium Technology for Fusion Reactors, CONF-750989, vol. I, USERDA, Gatlinburg, TN, 1976, p. 297.

[48] A.G. Pard, K.R. Garr, in: J.S. Watson, F.W. Wiffen (Eds.), Radiation Effects and Tritium Technology for Fusion Reactors, CONF-750989, vol. I, USERDA, Gatlinburg, TN, 1976, p. 312.
[49] B.N. Singh, J.H. Evans, A. Horsewell, P. Toft, D.J. Edwards, J. Nucl. Mater. 223 (1995) 95.
[50] V.K. Sikka, J. Moteff, J. Nucl. Mater. 46 (1973) 217.
[51] B.L. Eyre, Philos. Mag. 7 (1962) 2107.
[52] F.A. Smidt Jr., B. Mastel, Philos. Mag. 20 (1969) 651.
[53] N. Hashimoto, T.S. Byun, K. Farrell, S.J. Zinkle, J. Nucl. Mater. 336 (2005) 225.
[54] N. Hashimoto, T.S. Byun, K. Farrell, S.J. Zinkle, J. Nucl. Mater. 329–333 (2004) 947.
[55] T.S. Byun, N. Hashimoto, K. Farrell, E.H. Lee, J. Nucl. Mater., in press.